Acta Crystallographica Section B
**Structural Science**
ISSN 0108-7681

# Analyzing experimental electron density with the localized-orbital locator

**Vladimir Tsirelson[a]* and Adam Stash[b]**

[a]Mendeleev University of Chemical Technology, Miusskaya Sq. 9, Moscow 125047, Russia, and [b]Karpov Institute of Physical Chemistry, ul. Vorontsovo pole 10, 103064 Moscow, Russia

Correspondence e-mail: tsirel@muctr.edu.ru

Received 23 May 2002
Accepted 10 July 2002

The localized-orbital locator, which describes the features of bonding in terms of the local kinetic energy, is approximately expressed as a function of electron density and its first and second derivatives. Calculations based on accurate electron densities derived from X-ray diffraction data are carried out for crystals with different types of chemical bonds. It is demonstrated that the localized-orbital locator reveals the features of atomic interactions in a solid state and allows the covalent, ionic and van der Waals bonds to be distinguished.

## 1. Introduction

Recently, Schmider & Becke (2000, 2002) introduced the function

$$v(\mathbf{r}) = t(\mathbf{r})/[1 + t(\mathbf{r})], \tag{1}$$

which gives a measure of the relative velocity of electrons at a point $\mathbf{r}$ in the position space. The dimensionless variable

$$t(\mathbf{r}) = g_0(\mathbf{r})/g(\mathbf{r}) \tag{2}$$

depends on the positive definite one-electron kinetic energy density

$$g(\mathbf{r}) = (1/2)\sum_i \nabla\varphi_i(\mathbf{r})\nabla\varphi_i(\mathbf{r}), \tag{3}$$

where $\varphi_i(\mathbf{r})$ are the Hartree–Fock or Kohn–Sham orbitals. The kinetic energy density of a homogeneous electron gas with the density locally equal to the spinless electron density $\rho(\mathbf{r})$,

$$g_0(\mathbf{r}) = (3/10)(3\pi^2)^{2/3}[\rho(\mathbf{r})]^{5/3}, \tag{4}$$

provides a convenient reference level. Schmider & Becke (2000, 2002) noted that the kinetic energy density becomes small when a single dominating orbital has zero gradient, *i.e.* a localized orbital has a maximum or saddle point. Otherwise, it becomes large in the space between different localized orbitals. These features are mapped onto a function $v(1)$ with range $0 \leq v \leq 1$. Values of $v > 0.5$ indicate the regions where the electron's velocity is slower than that in a homogeneous electron-gas model ($v = 0.5$): these regions are associated with the localized orbitals describing the electron localization in covalent bonds and lone pairs. Values of $v < 0.5$ indicate the regions where electron kinetic energy is higher than that in a homogeneous electron gas: these regions are associated with ionic and van der Waals bonds with low electron density.

Function $v(1)$ reveals the localized electron locations without the explicit calculation of localized orbitals, hence Schmider & Becke (2000) named it the localized-orbital locator (LOL).

It is possible to derive the LOL without using the one-electron wave functions. Indeed, the kinetic energy density (1)

in the 'non-interactive' particle approximation can be rewritten in terms of the one-electron density matrix $\rho(\mathbf{r}, \mathbf{r}')$ as

$$g(\mathbf{r}) = (1/2) \sum_i \nabla \cdot \nabla \rho(\mathbf{r}, \mathbf{r}'). \quad (5)$$

The density matrix $\rho(\mathbf{r}, \mathbf{r}')$ is related to the one-particle Green function by the inverse Laplace transformation (Parr & Yang, 1989). Second-order gradient $\hbar$-expansion of the Green function around the classical Thomas–Fermi approximation (Kirzhnits, 1957) leads to the following approximate expression for kinetic energy density:

$$g_{\mathrm{DFT}}(\mathbf{r}) = (3/10)(3\pi^2)^{2/3}[\rho(\mathbf{r})]^{5/3} + |\nabla\rho(\mathbf{r})|^2 / [72\rho(\mathbf{r})] + [\nabla^2\rho(\mathbf{r})/6]. \quad (6)$$

This approximation, which is well known in the density functional theory (DFT) (Parr & Yang, 1989; Dreizler & Gross, 1990; Reznik, 1992), is suitable for the case of the smooth (but not necessary small) variation of electron density. Recently, Tsirelson (2002) found that approximation (6) provides the kinetic energy density calculated from the Hartree–Fock electron density, which is very close to the kinetic energy density calculated directly from Hartree–Fock wave functions. Therefore, in (2), we can replace the expression for $g(\mathbf{r})$ given in (3) by its approximate analogue (6). Now the modified expression for the LOL (we will denote it as $v_{\mathrm{DFT}}$) is dependent only on the electron density and its derivatives, making it unnecessary to use one-electron wave functions to calculate the LOL.

Approximation (6) violates the range of $v$, since $v_{\mathrm{DFT}}$ becomes negative near the nuclei owing to the discontinuity of the Laplacian term. The negative area has a maximum radius of 0.17 Å for the H atom; this radius is 0.02–0.05 Å for first-row atoms and even smaller for heavier atoms. We are mainly interested in the chemical-bond regions, therefore the regions around the nuclei may be omitted. Fortunately, no information is lost in this case: analysis of the behavior of the 'true' kinetic energy density (3) (Bader & Beddall, 1972) leads to the conclusion that $v$ always has a local maximum at the nuclei.

The aim of this work is to demonstrate that the modified LOL, calculated using expression (6) to approximate the kinetic energy density, is a useful tool for the analysis of experimental electron density. Recent advances in instrumentation and data treatment (Bolotovsky *et al.*, 1995; Graafsma *et al.*, 1997; Martin & Pinkerton, 1998; Boese *et al.*, 1999; Ivanov *et al.*, 1999; Tsirelson *et al.*, 2000) mean that single-crystal (X-ray, $\gamma$-ray, synchrotron) diffraction methods can provide a relatively accurate reconstruction of the electron density from the diffraction intensities with the help of the multipole structural model (Tsirelson & Ozerov, 1996). Although the model quasi-static electron density is not derived from the variational principle, it is close to the Hartree–Fock electron density. Moreover, it provides the kinetic energy density, as approximated by (6), which is in very reasonable agreement with the Hartree–Fock analogue for molecules and crystals with different types of chemical bonds (Tsirelson, 2002). This justifies the use of expression (6) in the LOL calculation.

**Table 1**
Positions of the extrema (Å) in the localized-orbital locator for krypton and strontium.

Free-atom values calculated using the approximate localized-orbital locator are listed in the first line, theoretical values by Schmider & Becke (2000) are given in the second line, and localized-orbital locator values derived from X-ray-diffraction data for bonded Kr along the Kr—Kr line in solid krypton and for bonded Sr along the Sr—O line in the $SrTiO_3$ crystal are given in the third line.

| | | Shell | | | | |
|---|---|---|---|---|---|---|
| Element | | *K* | *L* | *M* | *N* | *O* |
| Kr | $R_{\max}$ | 0† | 0.0581 | 0.2130 | 0.7939 | |
| | | 0 | 0.0661 | 0.2359 | 0.8284 | |
| | | 0 | 0.0615 | 0.2174 | 0.7596 | |
| | $R_{\min}$ | 0.0258 | 0.1291 | 0.4970 | $\infty$ | |
| | | 0.0287 | 0.1323 | 0.5041 | $\infty$ | |
| | | 0.0307 | 0.1313 | 0.4593 | 2.0493 | |
| Sr | $R_{\max}$ | 0† | 0.0554 | 0.2030 | 0.6828 | 2.2268 |
| | | 0 | 0.0619 | 0.2174 | 0.7646 | 2.2430 |
| | | 0 | 0.0553 | 0.1965 | 0.6817 | – |
| | $R_{\min}$ | 0.0246 | 0.1169 | 0.4368 | 1.4548 | $\infty$ |
| | | 0.0290 | 0.1233 | 0.4444 | 1.4890 | $\infty$ |
| | | 0.0246 | 0.1167 | 0.4360 | 1.5077 | – |

† Position of the first maximum in the LOL cannot be determined with the method under consideration (see text). Fortunately, this position is always known: it coincides with the nuclear position, where the LOL has a local maximum.

In this work, we have approximated the electron density for all compounds by the Hansen–Coppens (Hansen & Coppens, 1978) multipole model. The multipole parameters used in the calculations were taken from the following sources: Abramov & Okamura (1997) for Ge, Tsirelson *et al.* (1998) for LiF, Burgi *et al.* (2002) for benzene, Boese *et al.* (1997) and Bytheway *et al.* (2002) for ammonia, and Zhurova & Tsirelson (2002) for cubic perovskite $SrTiO_3$. Multipole parameters for Kr were derived using experimental data by Boese *et al.* (1999).[1] All calculations were performed using the program *WINXPRO* (Stash & Tsirelson, 2002).

## 2. Results

First, we studied the behavior of the approximate LOL, $v_{\mathrm{DFT}}$, in free atoms and found that it possesses alternating maxima and minima in exactly the same way as the original LOL of Schmider & Becke (2000). This reveals the structure of the electronic shells, reflecting electron concentration in the atomic shells and electron depletion between them. The LOL exhibits all the electronic shells for atoms with the outermost *s*- and *d*-shells, while the Laplacian of the electron density fails to distinguish the outer shells in some atoms, for example, the *M*- and *N*-shells in atoms from Sc to Ge *etc.* (Shi & Boyd, 1988; Sagar *et al.*, 1988). Table 1 lists the LOL extremum positions for a Kr atom with closed outermost *N*-electron shell and an Sr atom with two *s*-electrons in the outermost *O*-electron shell. The LOL exhibits four pairs of maxima and minima for Kr and five such pairs for Sr, in agreement with the numbers of their electronic shells. Corresponding LOL values for free atoms

[1] Boese *et al.* (1999) used the spherical-atom kappa model, not the multipole one.

calculated by Schmider & Becke (2000) using expressions (1)–(4) are also given in Table 1. Note that our LOL extrema lie systematically closer to the nucleus position because relativistic wave functions (Macchi & Coppens, 2001) were used in our calculations, while Schmider & Becke (2000) performed non-relativistic Hartree–Fock computations.

Next, we applied the modified LOL, $\nu_{\rm DFT}$, to reveal the features of the van der Waals bond in solid krypton, covalent bonds in crystalline germanium and benzene, and the ionic bond in lithium fluoride. The resulting LOL maps are presented in Figs. 1–3. We also calculated $\nu_{\rm DFT}$ in ammonia, $NH_3$, to test how the approximate LOL detects electron lone pairs (Fig. 4).

## 3. Discussion

There are two other functions – the Laplacian of the electron density (Bader, 1990) and the electron-localization function (Becke & Edgecombe, 1990; Savin *et al.*, 1991; Silvi & Savin, 1994) – that reveal the electron concentrations associated with the number and spatial arrangement of the localized electron pairs assumed in the VSEPR model (Gillespie & Hargittai, 1991). Both of these functions can be obtained from wave functions and parameters of the multipole model fitted to X-ray-diffraction structure factors (Tsirelson, 1996; Tsirelson & Stash, 2002). Therefore, they are used for interpretation of both theoretical and experimental electron densities. Recently, the electronic kinetic and potential local energies

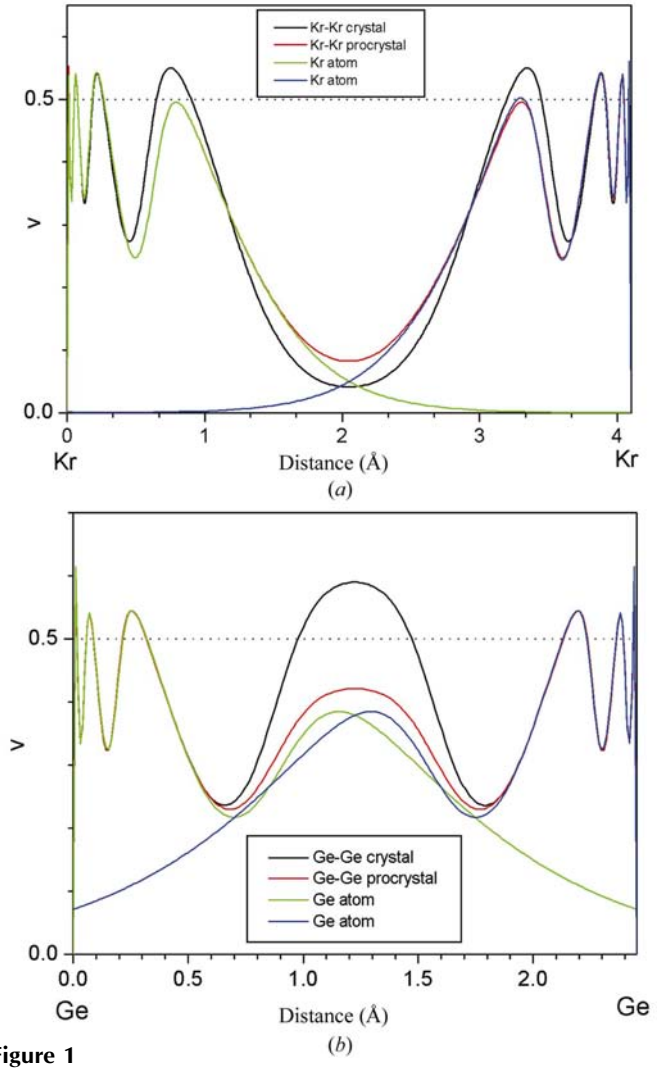


**Figure 1**
Profiles of the localized-orbital locator along the nearest interatomic lines in crystalline krypton (*a*) and germanium (*b*). Localized-orbital locator distributions for the procrystal as well as atomic contributions are depicted.

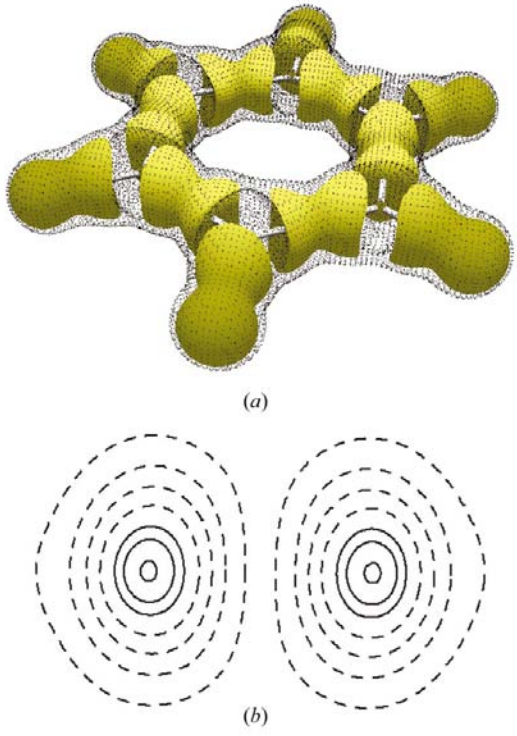


**Figure 2**
Localized-orbital locator in benzene, $C_6H_6$. (*a*) Electron concentrations are depicted by the yellow surfaces of $\nu_{\rm DFT} = 0.55$; the surface corresponding to $\nu_{\rm DFT} = 0.50$ is shown as a gray dotted net. A single molecule removed from a crystal is displayed. (*b*) Localized-orbital locator in the plane going through the middle-points of the C—C bonds; interval is 0.1 for $\nu_{\rm DFT} < 0.5$ (dashed lines) and 0.05 for $\nu_{\rm DFT} > 0.5$ (solid lines).

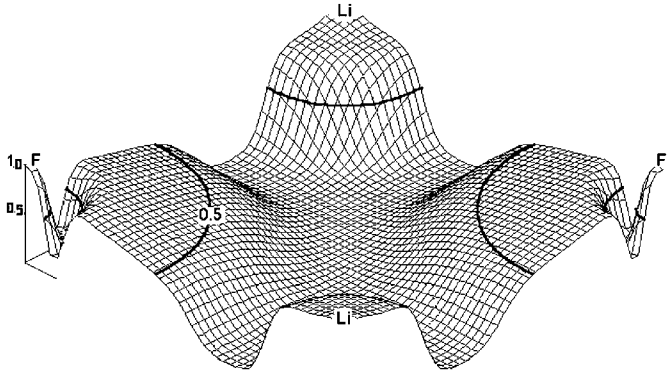


**Figure 3**
Distribution of the localized-orbital locator in a LiF crystal.

were also used to study bonding in molecules and crystals, and some interesting results were obtained with this approach (Espinosa *et al.*, 1998, 1999; Espinosa & Molins, 2000; Tsirelson, 2002; Zhurova *et al.*, 2002). The application of the LOL to the analysis of atomic interactions is similar. The LOL does not give quantitative results owing to the convenient but arbitrary choice of the homogeneous electron gas as the reference state. However, it simplifies the qualitative treatment of the bonding features for different types of atomic interactions. To demonstrate this, we consider the features of $\nu_{\rm DFT}$ in different compounds in more detail. We focus our attention on the electron-shell structure in solids in comparison with the shell structure in free atoms.

Kr and Ge atoms have the same number of electronic shells in a free state; however, Ge forms a crystal with covalent-bonded atoms, while Kr is crystallized at 99 K *via* closed-shell (van der Waals) atomic interactions. These crystals represent two extremes of bonding situations. In the Kr crystal (Fig. 1*a*), eight LOL maxima along the bond axis are separated by seven minima, with the deepest minimum situated in the middle of the Kr—Kr distance (positions of extrema in $\nu_{\rm DFT}$ for bonded Kr are given in Table 1). This implies that the outermost LOL minima inherent in the atoms have merged during crystallization. This may be written as MAX[(4+4)→8]/MIN[(4+4)→7], where (4+4) denotes the number of maxima/minima in a pair of interacting atoms and 8/7 denotes the resulting number of maxima/minima in a crystal. Comparison with a procrystal, a hypothetical system consisting of spherical non-interacting atoms placed in the positions of real atoms, shows (Fig. 1*a*) that an electron's velocity at the middle-bond point increases because of Pauli repulsion.

The LOL along the bond axis in the Ge crystal (Fig. 1*b*) exhibits seven maxima separated by six minima. The widest maximum lies at the middle of the Ge—Ge distance and corresponds to $\nu_{\rm DFT,max} = 0.526$. Thus, in contrast to crystalline Kr, the outermost LOL maxima inherent in Ge atoms have merged during the formation of the covalent bond, while the outermost atomic minima no longer exist. This situation may be written as MAX[(4+4)→7]/MIN[(4+4)→6]. We can conclude that the LOL distribution reflects the relative lowering of the kinetic energy density in the covalent bond in Ge, as seen by comparison with a procrystal (Fig. 2*b*), mainly because of constructive interference of the outermost atomic orbitals.

The non-polar covalent C—C bond in $C_6H_6$ exhibits a region of relatively large LOL values between the C atoms (Fig. 2*a*) centered at the middle-bond point. This region is separated from the atomic cores by minima, similar to the distribution in the Ge crystal. The LOL distribution in the plane perpendicular to the molecular plane at the middle of

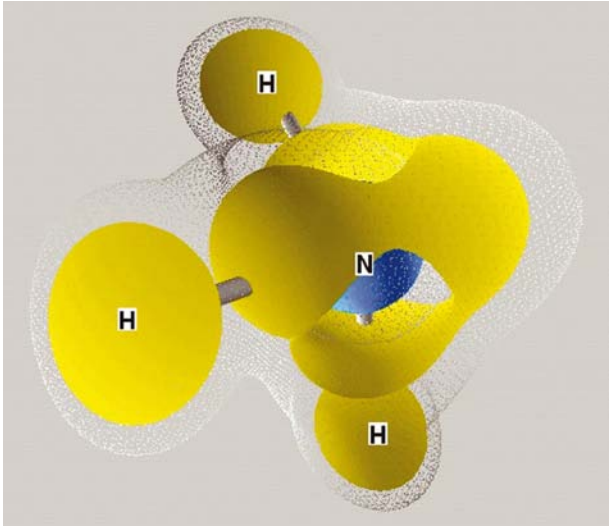


**Figure 4**
Distribution of the localized-orbital locator in the ammonia molecule removed from a crystal. Yellow surfaces correspond to $\nu_{\rm DFT} = 0.6$, while the surface $\nu_{\rm DFT} = 0.5$ is shown as a gray dotted net.

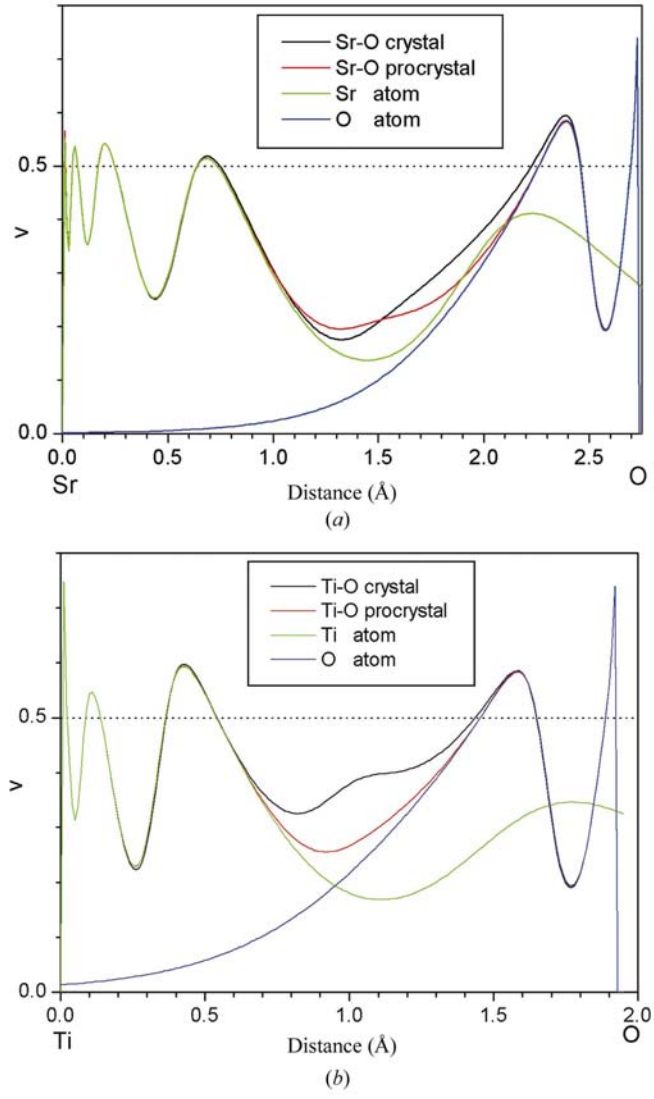


**Figure 5**
Profiles of the localized-orbital locator along the Sr—O (*a*) and Ti—O (*b*) lines in cubic perovskite $SrTiO_3$. Localized-orbital locator distributions for the procrystal as well as atomic contributions to the procrystal are depicted.

the C—C bond (Fig. 2*b*) shows an elongated area with $\nu_{DFT} > 0.5$. This displays the $\pi$-component of the C—C bond.

The covalent C—H bond lies almost entirely inside the region of the LOL with values $\nu_{DFT} > 0.5$; the maximum of the LOL is shifted from H to C atoms. The H atom is coreless, so the LOL minimum on the C—H bond behind the core of the C atom is very subtle.

Note that the surface $\nu_{DFT} = 0.5$ spans the skeleton of the whole molecule manifesting the electron's delocalization over the benzene circle.

The LOL in ammonia, $NH_3$ (Fig. 4), exhibits both bonding electrons on the N—H lines and concentration of electrons on the non-bonded orbital of *N* (electron lone pair). Thus, the relatively low kinetic energy density values are also typical for the lone-pair regions.

In a LiF crystal, the interionic charge transfer, as follows from the multipole refinement, is 0.97*e*: thus, the chemical bond in this crystal can be considered as ionic. In this crystal {MAX[(2+2)→3]/MIN[(2+2)→2] case}, the outer LOL maxima of atoms have merged, with the result that the maximum of the LOL on the Li—F line is shifted to fluorine (Fig. 3). Ions are well separated in space: the LOL values of $\nu_{DFT} \geq 0.5$ form practically spherical regions around each nucleus corresponding to near closed-shell ionic electron configurations in a solid state. In theoretical calculations (Schmider & Becke, 2000), a similar LOL pattern was found along the Li—F line in a single LiF molecule. The LOL value at a saddle point between the nearest ions in a crystal is $\nu_{DFT} = 0.09$, while the corresponding value for a molecule is about 0.15. This observation agrees with the fact that each ion in the LiF crystal has a much higher coordination number than that in the molecule. Note that the minimal LOL value at the interionic saddle point in LiF is close to that in the center of the Kr—Kr distance ($\nu_{DFT} = 0.05$): the relative kinetic energy density is high here in both compounds.

To better understand how LOL describes the polar covalent bond (the features of the bonds formed by coreless H atoms are not typical), we also calculated the LOL along the main bond lines in cubic perovskite $SrTiO_3$ (Fig. 5). The multipole-derived atomic charge distribution $Sr^{+0.31}Ti^{+1.6}O_3^{-0.63}$ (Zhurova & Tsirelson, 2002) shows that Sr and Ti ions give 0.14*e* and 0.40*e* in each Sr—O and Ti—O bond, respectively. Hence, the Sr—O bond is normally considered to be near ionic, whereas the Ti—O bond, as they believe, is a polar covalent bond (Tsirelson, 1999; Zhurova & Tsirelson, 2002). Indeed, the LOL distribution along the Sr—O bond resembles that in LiF: there is a deep well shaped minimum, the extreme point of which depends on the mutual size of the interacting atoms. The scheme of the electron-shell formation here is similar to that in LiF: MAX[(5+2)→6]/MIN[(5+2)→5]. The same type of electron-shell scheme takes place for the Ti—O bond, although the LOL distribution along the bond line is different: the LOL here has a tendency to form a plateau in the space between the two outer maxima. Correspondingly, the central minimum in this bond is smaller than that in the ionic Sr—O bond. Thus, the LOL allows the polar covalent and ionic bonds to be qualitatively distinguished.

## 4. Conclusions

The approach described above provides a calculation of the approximate localized-orbital locator, which exhibits features indicating the electron concentration and depletion in the position space. The treatment of the results obtained with accurate X-ray-diffraction analysis is significantly simplified and becomes closer to the quantum-chemical one. A covalent bond shows up a closed region of LOL values of more than 0.5 in internuclear space, while ionic and van der Waals atomic interactions exhibit closed regions of large LOL around nuclear positions and a saddle point (minimum) between them on the interatomic line. Electron lone pairs manifest themselves as local LOL maxima. It is significant that the localized-orbital locator distinguishes between not only the covalent, ionic and van der Waals bonds but also the polar covalent and ionic bonds. In this respect, it is superior to analysis based on the Laplacian of the electron density, which does not possess such an ability.

The authors thank Dr D. Yufit and Dr D. Jayatilaka for providing the experimental data for benzene and ammonia, and Professor I. D. Brown for discussion.

## References

Abramov, Yu. A. & Okamura, F. P. (1997). *Acta Cryst.* A**53**, 187–198.
Bader, R. F. W. (1990). *Atoms in Molecules: A Quantum Theory.* Oxford: Clarendon Press.
Bader, R. F. W. & Beddall, P. M. (1972). *J. Chem. Phys.* **56**, 3320–3329.
Becke, A. D. & Edgecombe, K. E. (1990). *J. Chem. Phys.* **92**, 5397–5403.
Boese, R., Blaeser, D., Heinemann, O., Abramov, Yu., Tsirelson, V., Blaha, P. & Schwarz, K. (1999). *J. Phys. Chem.* A**103**, 6209–6213.
Boese, R., Niederpruem, N., Blaeser, D., Maulitz, A., Antipin, M. & Mallinson, P. R. (1997). *J. Phys. Chem.* B**101**, 5794–5799.
Bolotovsky, R., Darovsky, A., Kezerazhvili, V. & Coppens, P. (1995). *J. Appl. Cryst.* **28**, 86–95.
Burgi, H.-B., Capelli, S., Goeta, A. E., Howard, J. A. K., Spackman, M. A. & Yufit, D. S. (2002). *Chem. Eur. J.* In the press.
Bytheway, I., Grimwood, D. J., Figgis, B. N., Chandler, G. N. & Jayatilaka, D. (2002). *Acta Cryst.* A**58**, 244–251.
Dreizler, R. M. & Gross, E. K. U. (1990). *Density Functional Theory.* Berlin: Springer-Verlag.
Espinosa, E., Lecomte, C. & Molins, E. (1999). *Chem. Phys. Lett.* **300**, 745–748.
Espinosa, E. & Molins, E. (2000). *J. Chem. Phys.* **11**, 5686–5694.
Espinosa, E., Molins, E. & Lecomte, C. (1998). *Chem. Phys. Lett.* **285**, 170–173.
Gillespie, R. J. & Hargittai, I. (1991). *The VSEPR Model of Molecular Geometry.* Englewood Cliffs, NJ: Prentice Hall.
Graafsma, H., Svensson, S. O. & Kvick, Å. (1997). *J. Appl. Cryst.* **30**, 957–962.
Hansen, N. & Coppens, P. (1978). *Acta Cryst.* A**34**, 909–921.
Ivanov, Y., Zhurova, E. A., Zhurov, V. V., Tanaka, K. & Tsirelson, V. G. (1999). *Acta Cryst.* B**55**, 923–930.
Kirzhnits, D. A. (1957). *Sov. Phys. JETP*, **5**, 64–72.
Macchi, P. & Coppens, P. (2001). *Acta Cryst.* A**57**, 656–662.
Martin, A. & Pinkerton, A. A. (1998). *Acta Cryst.* B**54**, 471–477.
Parr, R. G. & Yang, W. (1989). *Density-Functional Theory of Atoms and Molecules*. New York: Oxford University Press.
Reznik, I. M. (1992). *Electron Density Theory of the Ground State Properties of Crystals.* Kiev: Naukova Dumka.

Sagar, R. P., Ku, A. C. T., Smith, V. H. & Simas, A. M. (1988). *J. Chem. Phys.* **88**, 4367–4374.
Savin, A., Becke, A. D., Flad, J., Nesper, R., Press, H. & von Schnering, H. G. (1991). *Angew. Chem. Int. Ed. Engl.* **30**, 409–410.
Schmider, H. L. & Becke, A. D. (2000). *J. Mol. Struct.* (*Theochem*), **527**, 51–61.
Schmider, H. L. & Becke, A. D. (2002). *J. Chem. Phys.* **116**, 3184–3193.
Shi, Z. & Boyd, R. J. (1988). *J. Chem. Phys.* **88**, 4375–4377.
Silvi, B. & Savin, A. (1994). *Nature* (*London*), **371**, 63–67.
Stash, A. & Tsirelson, V. (2002). *J. Appl. Cryst.* **35**, 371–373.
Tsirelson, V. (1996). *Can. J. Chem.* **74**, 1171–1179.
Tsirelson, V. (2002). *Acta Cryst.* B**58**, 632–639.
Tsirelson, V. & Stash, A. (2002). *Chem. Phys. Lett.* **351**, 142–148.
Tsirelson, V. G. (1999). *Acta Cryst.* A**55** Supplement, Abstract M13.OF.003.
Tsirelson, V. G., Abramov, Yu. A., Zavodnik, V. E., Stash, A. I., Belokoneva, E. L., Stahn, J., Pietsch, U. & Feil, D. (1998). *Struct. Chem.* **9**, 249–254.
Tsirelson, V. G., Ivanov, Yu., Zhurova, E. A., Zhurov, V. V. & Tanaka, K. (2000). *Acta Cryst.* B**56**, 197–203.
Tsirelson, V. G. & Ozerov, R. P. (1996). *Electron Density and Bonding in Crystals.* Bristol/Philadelphia: Institute of Physics.
Zhurova, E. A. & Tsirelson, V. G. (2002). *Acta Cryst.* B**58**, 567–575.
Zhurova, E. A., Tsirelson, V. G., Stash, A. I. & Pinkerton A. A. (2002). *J. Am. Chem. Soc.* **124**, 4574–4575.